Future Changes in the Impact of North Pacific Midlatitude Oceanic Frontal Intensity on the Wintertime Storm Track in CMIP5 Models

Yao YAO[1], Zhong ZHONG[1,2*], Xiu-Qun YANG[2], and Xiaogang HUANG[3]

1 *College of Meteorology and Oceanography*, *National University of Defense Technology*, *Changsha* 410073
2 *Jiangsu Collaborative Innovation Center for Climate Change*, *School of Atmospheric Sciences*, *Nanjing University*, *Nanjing* 210023
3 *Army Academy of Artillery and Air Defense (Nanjing Campus)*, *Nanjing* 211132

(Received April 24, 2020; in final form September 20, 2020)

ABSTRACT

The storm track and oceanic front play an important role in the midlatitude air–sea interaction. In this study, future changes in the impact of the North Pacific midlatitude oceanic frontal intensity on the wintertime storm track are projected based on climate model outputs from the Coupled Model Intercomparison Project Phase 5 (CMIP5). The performance of 13 CMIP5 models is evaluated, and it is found that a majority of these models are capable of reproducing the northward intensification of the storm track in response to the strengthened oceanic front. The ensemble means of outputs from six best models under three Representative Concentration Pathway (RCP) scenarios (RCP2.6, RCP4.5, and RCP8.5) are compared with the results of the historical simulation, and future changes are projected. It is found that the impact of the oceanic frontal intensity on the storm track tends to get stronger and extends further westward in a warming climate, and the largest increase appears in the RCP8.5 run. Further analysis reveals that the stronger impact of the oceanic front on the storm track in the future may be partially attributed to the greater oceanic frontal impact on the near-surface baroclinicity, which is mainly related to the intensified oceanic frontal impact on the meridional potential temperature gradient under the climate change scenario. However, this process can hardly explain the increasing impact of the oceanic front on the upstream of the storm track.

Key words: storm track, midlatitude oceanic front, climate change, Coupled Model Intercomparison Project Phase 5 (CMIP5)

Citation: Yao, Y., Z. Zhong, X.-Q. Yang, et al., 2020: Future changes in the impact of North Pacific midlatitude oceanic frontal intensity on the wintertime storm track in CMIP5 models. *J. Meteor. Res.*, **34**(6), 1199–1213, doi: 10.1007/s13351-020-0057-z.

1. Introduction

Storm tracks refer to regions where synoptic scale transient eddies are active and intense (Blackmon, 1976; Blackmon et al., 1977; Chang et al., 2002). Cyclones and anticyclones moving along the storm track not only affect severe weather including extreme precipitation (Pfahl and Wernli, 2012a; Chen et al., 2013b), strong winds (Booth et al., 2010), and extremely high/low temperature (Pfahl and Wernli, 2012b; Chen et al., 2013a; Zhou et al., 2015; Chang et al., 2016), but also influence the midlatitude climate system via the systematic transport of the momentum, heat, and water vapor (Wettstein and Wallace, 2010; Ma and Zhang, 2018; Chu et al., 2020).

In North Pacific, warm water from the Kuroshio and cold water from the Oyashio converge near 40°N, forming a meridionally narrow region with the intense meridional sea surface temperature (SST) gradient, which is the so-called midlatitude oceanic front (Nakamura and Kazmin, 2003). Nakamura et al. (2004) found that the storm track is always present over the midlatitude oceanic front, implying a close relationship between the two. Based on a set of idealized model experiments, Nakamura et al. (2008) and Sampe et al. (2010) argued that the sensible heat flux difference across the oceanic frontal zone effectively maintains the near-surface baroclinicity and thereby anchoring the storm track, a process referred

Supported by the National Natural Science Foundation of China (42005025), Scientific Research Fund of National University of Defense Technology (ZK20-34), and "Double-First Class" Special Fund of National University of Defense Technology (qnrc01).

*Corresponding author: zhong_zhong@yeah.net.

to as the "oceanic baroclinic adjustment" mechanism. Recently, observational and numerical studies generally indicate that the midlatitude oceanic front can significantly affect the storm track by modulating the near-surface baroclinicity (Taguchi et al., 2009; Small et al., 2014; Yao et al., 2016), and thus regulating the midlatitude atmospheric circulation via transient eddy forcing (Fang and Yang, 2016; Wang et al., 2019; Huang et al., 2020). Therefore, the oceanic front and the storm track play an important role in the midlatitude air–sea interaction (Small et al., 2008; Frankignoul et al., 2011; Gan and Wu, 2013; Yao et al., 2017, 2018b; Omrani et al., 2019).

In the past decade or so, much attention has been paid to future changes in the storm track and midlatitude oceanic front under the climate change. Most of the previous studies have reached a consensus that the storm track in the Northern Hemisphere will shift poleward and expand upward, while the storm frequency will decrease in midlatitudes (Yin, 2005; Chang et al., 2012; Zhang and Ding, 2014; Tamarin-Brodsky and Kaspi, 2017). Harvey et al. (2012) pointed out that the magnitude of the storm track response to climate change simulated by individual models is typically of the order of interdecadal variation, and locally can be as large as the interannual variation. Additionally, the western boundary currents are projected to intensify and move northward, which may cause similar changes in the midlatitude oceanic front (Seager and Simpson, 2016; Yang et al., 2016; Li et al., 2017). Zhang et al. (2017) found that wind stress changes and ocean stratification changes both contribute to the enhancement of the Kuroshio Extension.

As illustrated above, respective changes in the storm track and midlatitude oceanic front under global warming have recently been studied in depth. However, possible changes of their relationship have not been investigated. Since the North Pacific oceanic front and storm track play an important role in shaping the midlatitude climate, it is of great significance to understand how the impact of the oceanic front on the storm track will change in a warming climate. Based on model outputs from the Coupled Model Intercomparison Project Phase 5 (CMIP5; Taylor et al., 2012), this study aims to address two questions: (1) Are CMIP5 models capable of simulating the impact of the North Pacific oceanic frontal intensity on the wintertime storm track? (2) How will the impact change in a warming climate?

This paper is organized as follows. Section 2 introduces the data and methods implemented in this study. Section 3 evaluates the performance of CMIP5 models in reproducing the North Pacific midlatitude oceanic front and its impact on the wintertime storm track. In Section 4, future changes are projected and the potential mechanism is analyzed based on the multi-model ensemble results of six best models (6BMME). Conclusions and discussion are presented in the last section.

2. Data and methods

2.1 *Model data*

Outputs from the following 13 CMIP5 models are considered in this study: CanESM2, CNRM-CM5, CSIRO-Mk3.6.0, GFDL-CM3, GFDL-ESM2G, GFDL-ESM2M, IPSL-CM5A-LR, IPSL-CM5A-MR, MIROC5, MIROC-ESM-CHEM, MPI-ESM-LR, MPI-ESM-MR, and MRI-CGCM3 (Taylor et al., 2012). Future changes are determined by comparing the present-day simulations (1980–2004) and future climate simulations (2075–2099) under three Representative Concentration Pathway (RCP) scenarios (RCP2.6, RCP4.5, and RCP8.5), which correspond to the 2.6-, 4.5-, and 8.5-W m^{-2} radiative forcings by 2100, respectively (Moss et al., 2010; Meinshausen et al., 2011; Van Vuuren et al., 2011).

2.2 *Observations*

The daily meridional wind, monthly mean temperature, and geopotential height are derived from the NCEP–NCAR global 2.5°×2.5° reanalysis product (Kalnay et al., 1996). The monthly mean SST is obtained from the Met Office Hadley Centre Sea Ice and SST version 1 data (HadISST1; Rayner et al., 2003) on global 1° × 1° grids. The NCEP–NCAR reanalysis data and HadISST1 SST over the period of 1980–2004 are taken as "observations" to compare with the CMIP5 historical simulations. To facilitate comparisons with observations, all the CMIP5 atmospheric data are interpolated to the NCEP–NCAR 2.5° × 2.5° grids, and the CMIP5 SST data are interpolated to the HadISST1 1° × 1° grids.

2.3 *Methods*

The storm track in the upper, middle, and lower tropospheres is measured by the 2–8-day bandpass filtered meridional velocity variance at 250, 500, and 700 hPa ($v'v'_{250}$, $v'v'_{500}$, and $v'v'_{700}$), respectively (Blackmon et al., 1977; Chang and Fu, 2002; Gan and Wu, 2013). The Eady growth rate at 850 hPa (σ_{850}) is used to represent the near-surface baroclinicity. It can be expressed by $\sigma = -0.31 g N^{-1} \theta^{-1} (\partial\theta/\partial y)$, where θ is the potential temperature, g is the gravity acceleration, and N is the Brunt-Väisälä frequency (Lindzen and Farrell, 1980; Nakamura and Yamane, 2010).

Following Yuan and Xiao (2017), an oceanic frontal intensity index (I_{OF}) is defined as the normalized SST meridional gradient ($-\partial \mathrm{SST}/\partial y$) averaged over

35°–45°N, 145°E–180°, where the intensity and variance of the SST meridional gradient are relatively large. The linear regression analysis is applied to investigate the influence of the oceanic frontal intensity on the storm track. Prior to the regression analysis, anomalies of atmospheric variables are obtained first by removing their climatological means and linear trends. Here, winter refers to as December, January, and February in the Northern Hemisphere.

To objectively evaluate the CMIP5 models' performance, we calculate the pattern correlation coefficient (PCC) between observations and historical simulations. A high positive PCC indicates good performance of the model in reproducing the spatial pattern of the variable, while a low PCC indicates poor performance (Booth et al., 2017).

3. Evaluation and selection of CMIP5 models

3.1 *Simulation of the wintertime midlatitude oceanic front*

Figure 1 displays the wintertime SST and its meridional gradient from the HadISST1 data and outputs of 13 CMIP5 models. The observation shows intense meridional SST gradients to the east of Japan, with the maximum extending along 40°N. All the 13 models can basically capture the spatial pattern and meridional position of the wintertime midlatitude oceanic front. Among these models, IPSL-CM5A-MR performs the best with the PCC up to 0.840. The oceanic frontal intensities simulated by CNRM-CM5, GFDL-CM3, GFDL-ESM2G, GFDL-ESM2M, MPI-ESM-MR, and MRI-CGCM3 are relatively stronger than the observation, which might be attributed to the relatively high resolutions used in these models because more detailed structure of the oceanic front can be distinguished at higher resolution. Additionally, all the models can reproduce the interannual variance pattern of the meridional SST gradient, and the largest variance is basically consistent with its climatological maximum (figure omitted). Note that since all the models have the ability to simulate the wintertime midlatitude oceanic front and there are no relatively large inter-model differences, the oceanic frontal intensity index defined in the fixed domain (35°–45°N, 145°E–180°) is reasonable, where the intensity and variance of the SST meridional gradient are relatively large in both the observation and historical model simulations.

3.2 *Simulation of the impact of the oceanic frontal intensity on the storm track*

In order to investigate the impact of the oceanic frontal intensity on the storm track, the storm-track anomalies are regressed on I_{OF}. Figures 2–4 display the storm-track regressions in the upper, middle, and lower troposphere. Historical simulations are compared to the observation to gain confidence in using the CMIP5 models for future projections. Figure 5 shows the PCC of storm-track regressions.

In the observation, when the oceanic front strengthens, the storm track in the three tropospheric levels exhibits significant positive anomalies to the north of the climatological maximum and weak negative anomalies to the south, which indicates a northward intensification of the storm track corresponding to the strengthened oceanic front (Figs. 2a, 3a, 4a). For the upper-level storm track, except CSIRO-Mk3.6.0, GFDL-CM3, GFDL-ESM2G, and GFDL-ESM2M, the other nine models can well reproduce the observed northward intensification of the storm track (Figs. 2b–n). Among them, CNRM-CM5 bears the closest resemblance to the storm-track anomalous pattern shown in the observation, with the PCC reaching up to 0.665 (Fig. 5; green curve). It is worth noting that although IPSL-CM5A-MR, MIROC5, MPI-ESM-LR, and MPI-ESM-MR slightly overestimate the impact of the oceanic front, these models still demonstrate skills of simulating the storm-track anomalous pattern associated with the oceanic front. For the mid-level storm track, except CSIRO-Mk3.6.0 and GFDL-CM3, all the other 11 models can simulate the storm-track anomalous pattern, and MPI-ESM-LR performs the best with the PCC up to 0.701 (Figs. 3b–n, 5; blue curve). Similarly, although GFDL-ESM2G, MPI-ESM-LR, and MPI-ESM-MR overestimate the impact of the oceanic front, they still have the ability to reproduce the spatial pattern of the oceanic frontal impact. For the lower-level storm track, except CSIRO-Mk3.6, GFDL-CM3, IPSL-CM5A-LR, MIROC5, and MPI-ESM-MR, the other eight models perform well in describing the storm-track anomalies associated with the oceanic front, and MPI-ESM-LR performs the best with the PCC up to 0.587 (Figs. 4b–n, 5; yellow curve). It is clear that most models can reasonably reproduce the oceanic frontal impact on the storm track in the upper and middle troposphere, which may be partially related to the relatively weak impact on the storm track in the lower troposphere.

Therefore, despite of certain biases in representing the amplitude of the storm-track regression, most of the 13 CMIP5 models have skills of reproducing the storm-track anomalous pattern associated with the oceanic frontal intensity. This result indicates that most models are capable of simulating the impact of the oceanic frontal intensity on the storm track.

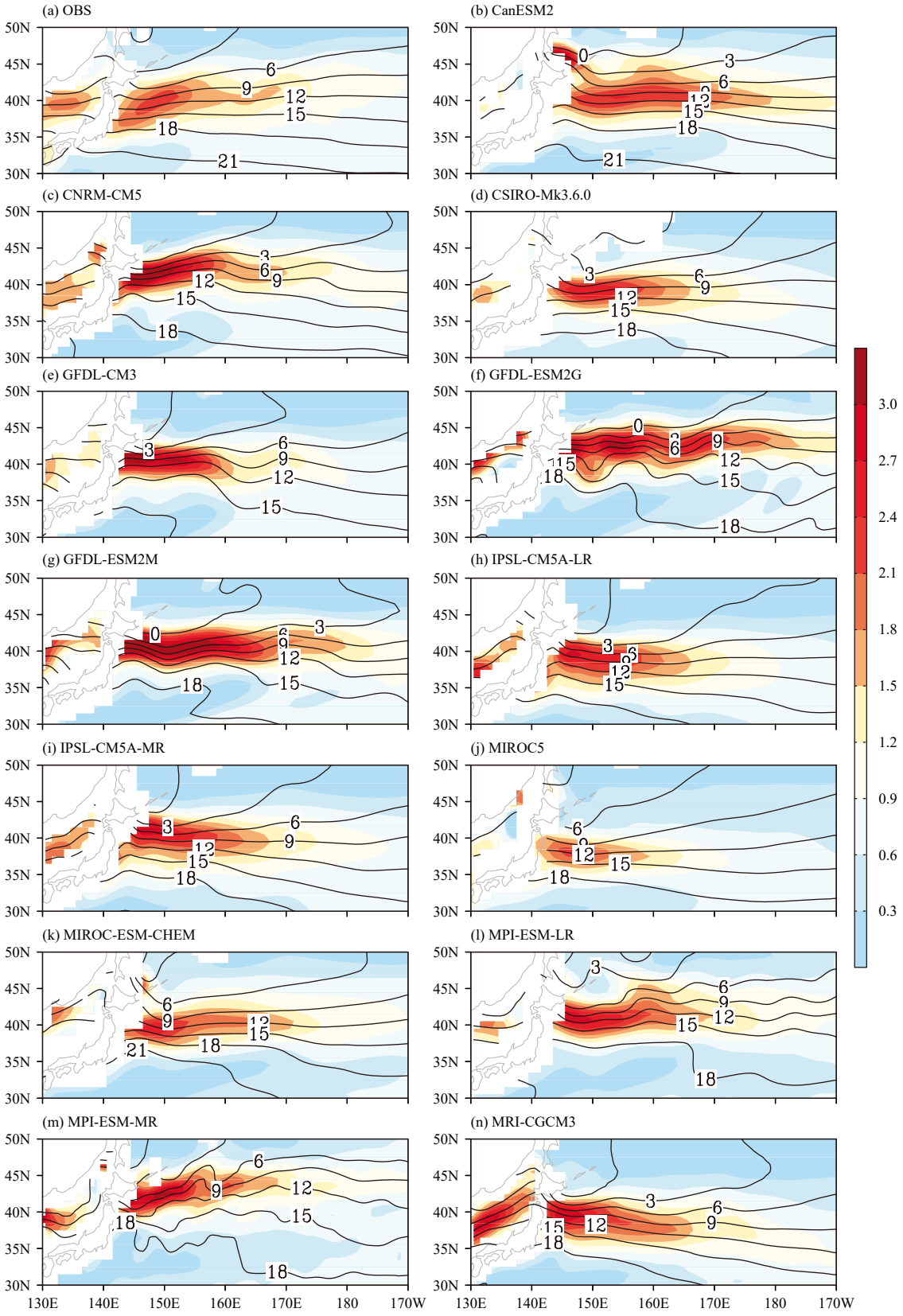

Fig. 1. Wintertime SST (contour; °C) and its meridional gradient [shading; °C (100 km)$^{-1}$] in the (a) observation (OBS) and (b–n) CMIP5 model historical simulations.

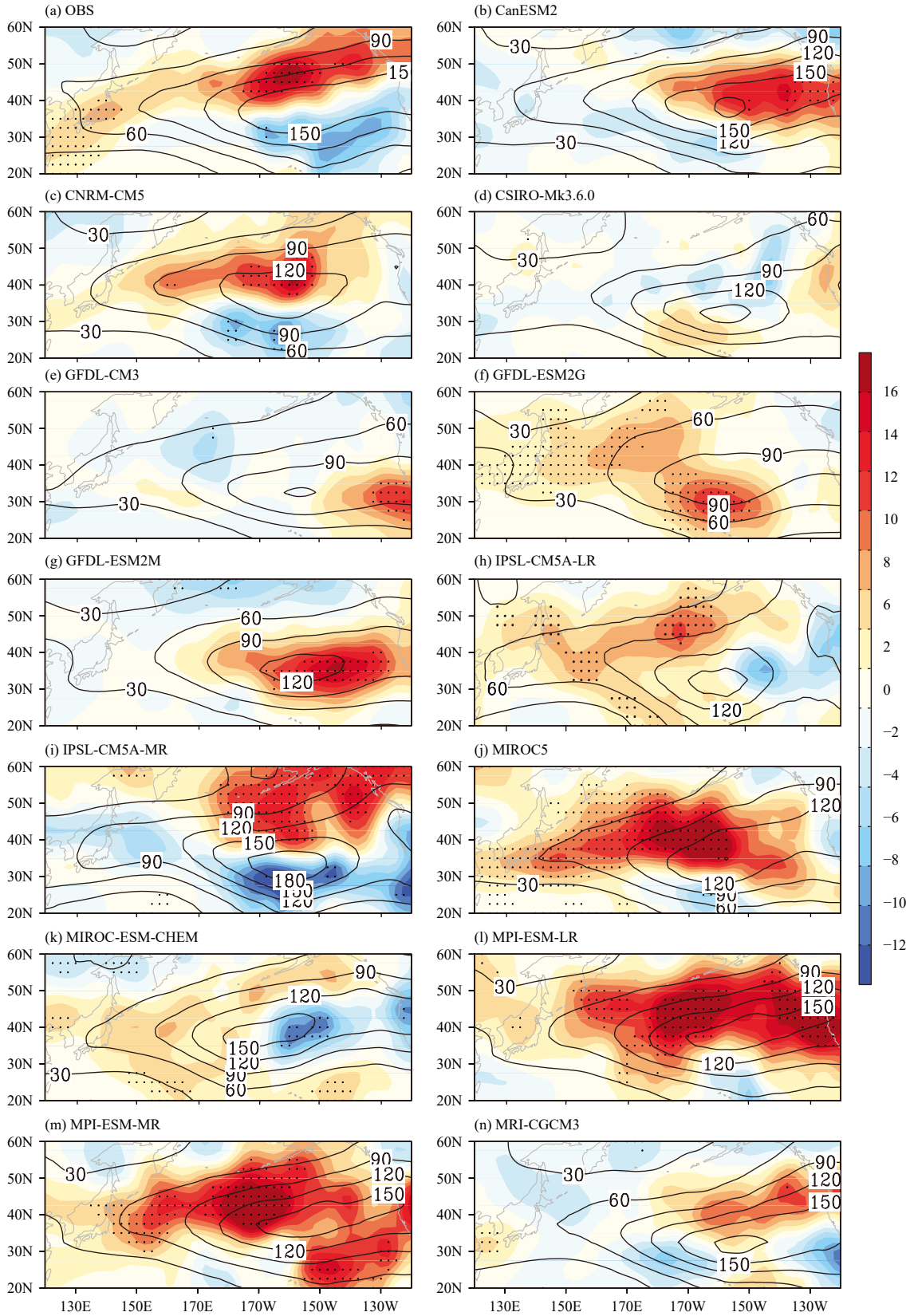

Fig. 2. Wintertime storm track at 250 hPa (contour; $m^2\ s^{-2}$) and its anomalies regressed upon the oceanic frontal intensity index I_{OF} (shading; $m^2\ s^{-2}$) in the (a) observation (OBS) and (b–n) CMIP5 model historical simulations. Stippling denotes the regions passing the Student's *t*-test at the 95% confidence level.

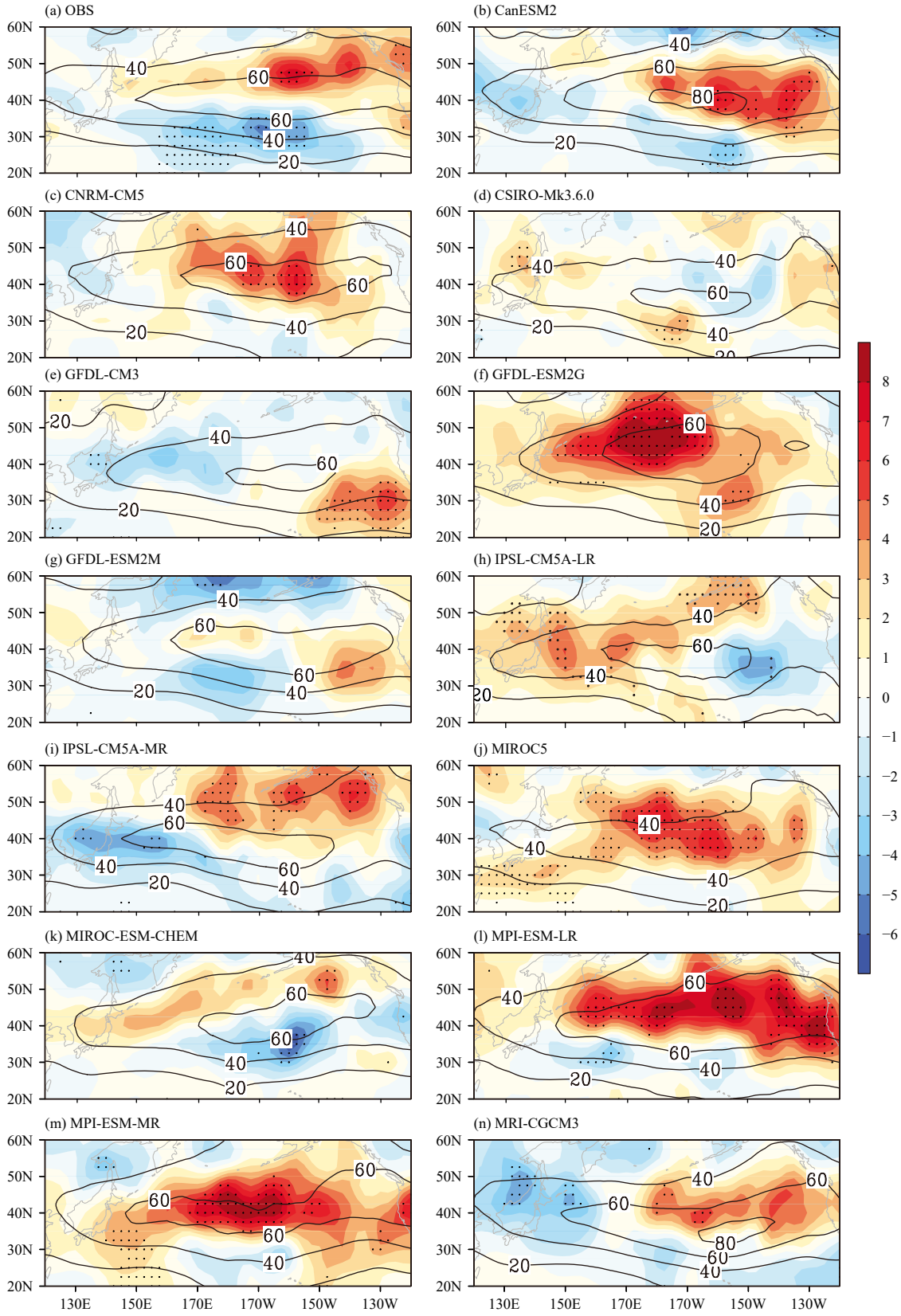

Fig. 3. As in Fig. 2, but for storm track at 500 hPa.

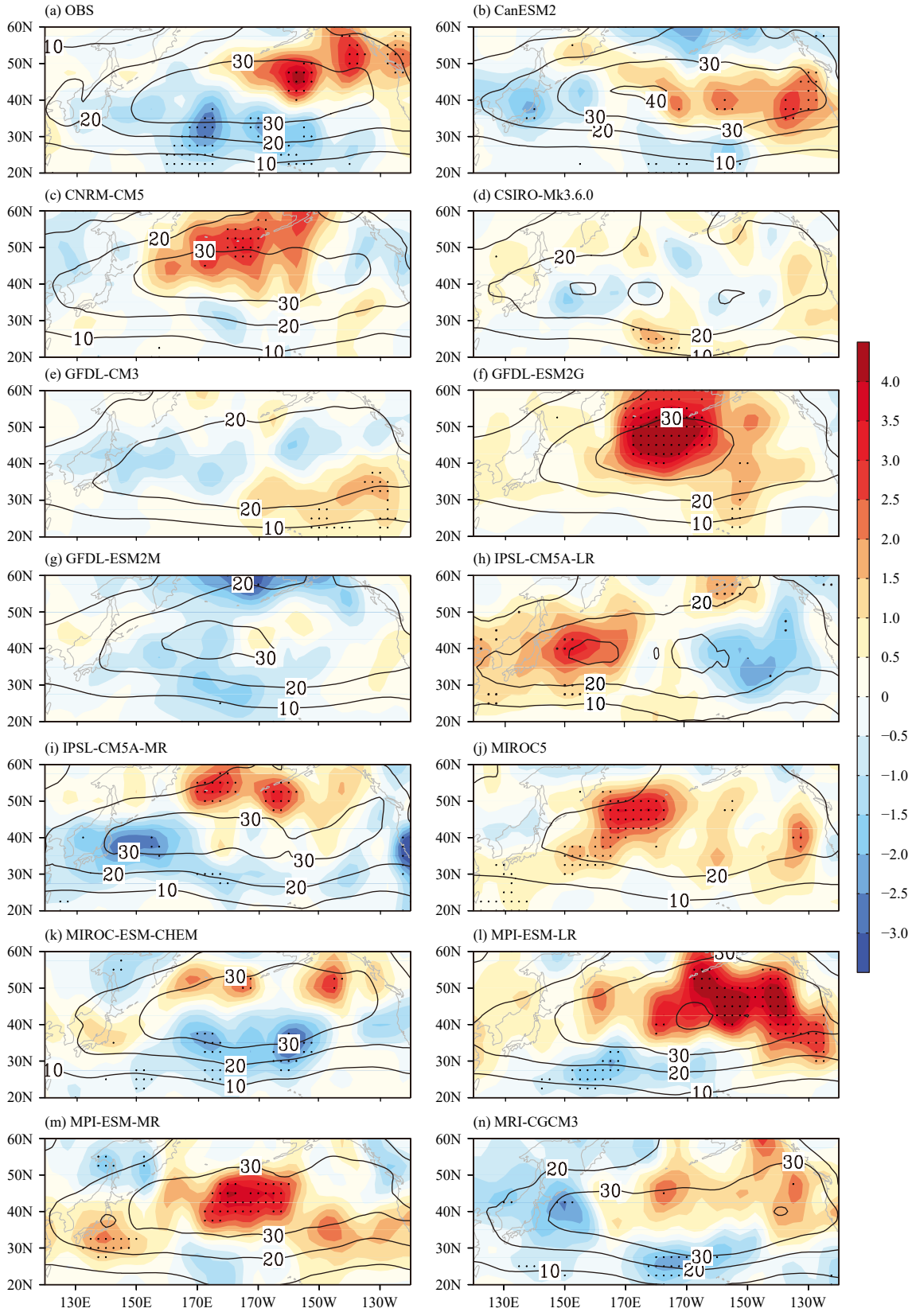

Fig. 4. As in Fig. 2, but for storm track at 700 hPa.

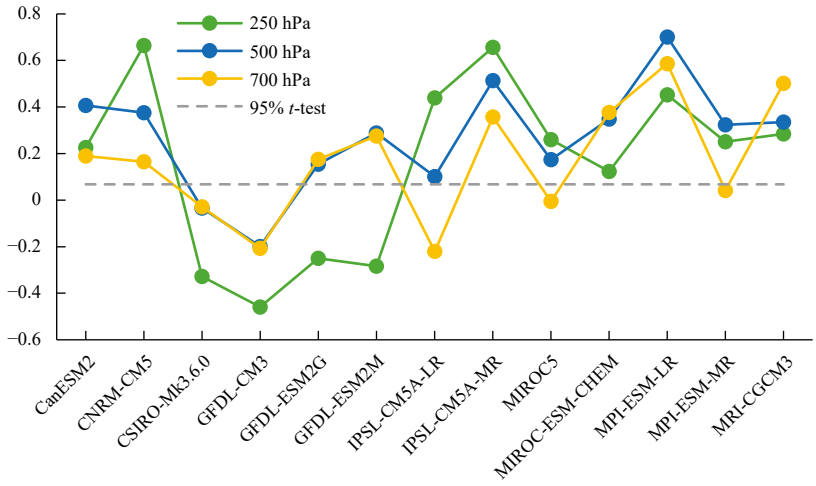

Fig. 5. The pattern correlation coefficient (PCC) between the observation and individual model simulation for the storm-track regression upon I_{OF} (absolute values larger than 0.068 are significant at the 95% confidence level based on Student's *t*-test).

3.3 *Best model selection*

Based on the models' performance in representing the impact of the oceanic frontal intensity on the storm track, we select several best models for further analysis of future changes. A model is chosen as the best model if the PCC of the storm-track regression in the upper, middle, and lower tropospheres are all positive and statistically significant. Based on this criterion, six best models are selected, i.e., CanESM2, CNRM-CM5, IPSL-CM5A-MR, MIROC-ESM-CHEM, MPI-ESM-LR, and MRI-CGCM3 (Fig. 5). The 6BMME is utilized for the future projection. It is worth noting that the CMIP5 models may have interdependencies among them (Knutti et al., 2013), which may affect the significance of results (Sanderson et al., 2015). However, the models used for producing the 6BMME are relatively independent.

4. Future changes in the impact of oceanic frontal intensity on storm track

4.1 *Future projection from multi-model ensemble*

In this subsection, we analyze future changes in the impact of the oceanic frontal intensity on the storm track by comparing the 6BMME under each RCP scenario (2075–2099) with that in the historical run (1980–2004). Figure 6 shows the 6BMME of the storm track and its anomalies regressed upon I_{OF} in the historical and RCP2.6 runs, as well as differences in the storm-track regression between the historical and RCP2.6 runs. Similarly, the results for the RCP4.5 and RCP8.5 runs are exhibited in Figs. 7, 8, respectively.

In the RCP2.6 run, when the oceanic front strengthens, the storm track exhibits positive anomalies in the central part of its climatological region, indicating that the storm track intensifies in response to the enhanced oceanic front (Figs. 6b, e, h). Compared with the historical run, the storm-track regression increases in the central part and upstream of the storm track but decreases in the north, which suggests that the impact of the oceanic front on the storm track gets stronger and extends further westward but becomes weaker in the north (Figs. 6c, f, i). It seems that the future increase in the oceanic frontal impact on the storm track is larger in the upper troposphere than that in the middle and lower tropospheres.

Similar to that in the historical run, the storm track in the RCP4.5 run intensifies northward as the oceanic front strengthens (Figs. 7b, e, h). However, the storm-track regression is larger in the central part and upstream of the storm track (Figs. 7c, f, i), suggesting that the impact of the oceanic front tends to become more robust and extends further westward as the RCP2.6 run. The increase in the oceanic frontal impact is also much larger in the upper level than that in other levels.

Similar to that in the historical run, the storm track in the RCP8.5 run exhibits a northward intensification as the oceanic front increases (Figs. 8b, e, h), and the storm-track regression is much larger, especially in the upstream of the storm track (Figs. 8c, f, i). In the upper troposphere, the oceanic frontal impact becomes stronger in both the central part and upstream of the storm track, while the increase is more significant in the upstream of the middle and lower tropospheres. As expected, the future changes are the largest in the RCP8.5 run than that in the RCP2.6 and RCP4.5 runs, indicating that the impact of the oceanic front on the storm track is the strongest and extends the farthest westward in the

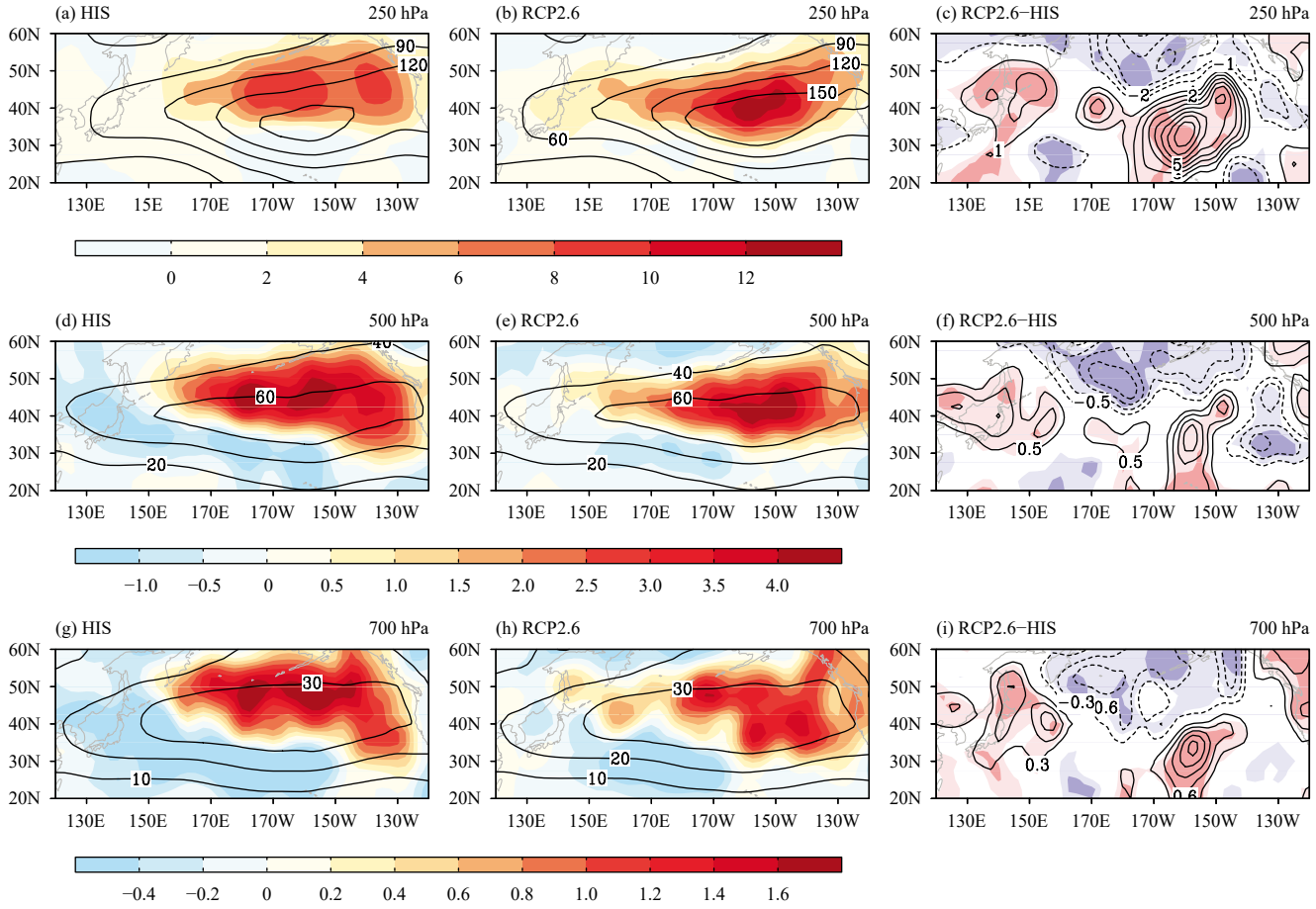

Fig. 6. The multi-model ensemble of the wintertime storm track from outputs of six best models (contour; $m^2\ s^{-2}$) and storm-track anomalies regressed upon I_{OF} (shading; $m^2\ s^{-2}$) in the historical (left panels) and RCP2.6 runs (middle panels). Differences in the storm-track regression (contour; $m^2\ s^{-2}$) between RCP2.6 and historical runs are shown in the right panels, the areas shaded in red and blue denote positive and negative changes respectively, and the light (dark) shading indicates that more than three (four) of six best models agree on the sign of the projected change. The storm tracks at (a–c) 250 hPa, (d–f) 500 hPa, and (g–i) 700 hPa are displayed.

RCP8.5 run.

Figure 9 displays the storm-track regression area-averaged over 30°–50°N, 130°E–130°W, in the historical and three RCP runs, and the corresponding changing rates in the future relative to present are shown in Table 1. In the lower and middle troposphere, the oceanic frontal impact tends to become stronger as the radiative forcing becomes larger. That is, the impact is the largest (smallest) in the RCP8.5 (RCP2.6) run. Specifically, the storm-track regression in the lower (middle) troposphere will increase by approximately 41.5% (11.86%) in the RCP2.6 run and approximately 106.03% (59.31%) in the RCP8.5 run. Similarly, in the upper troposphere, the largest impact of the oceanic front appears in the RCP8.5 run, whereas the changing rate is not proportional to the RCP radiative forcing, which is relatively small in the RCP4.5 run (39.31%) compared with those in the RCP2.6 (42.94%) and RCP8.5 (72.16%) runs. The above analysis suggests that the impact of the oceanic front on the storm track will become stronger and extend further westward in a warming climate, with the largest increase appearing in the RCP8.5 run.

4.2 *Possible mechanism responsible for future changes*

As demonstrated in previous studies, the midlatitude oceanic front affects storm track activities mainly through changing the near-surface baroclinicity (Yao et al., 2018a, 2019), and therefore future changes in the impact of the oceanic front on the storm track is probably related to the changes in the near-surface baroclinicity anomalies associated with the oceanic front. Figure 10 shows the 6BMME of the near-surface baroclinicity and its anomalies regressed upon I_{OF} in each RCP run, as well as the differences in the regression between the RCP and historical runs. In each RCP run, when the oceanic front strengthens, the near-surface baroclinicity increases to the north of the climatological peak (Figs. 10a–c), which is favorable for the northward intensifica-

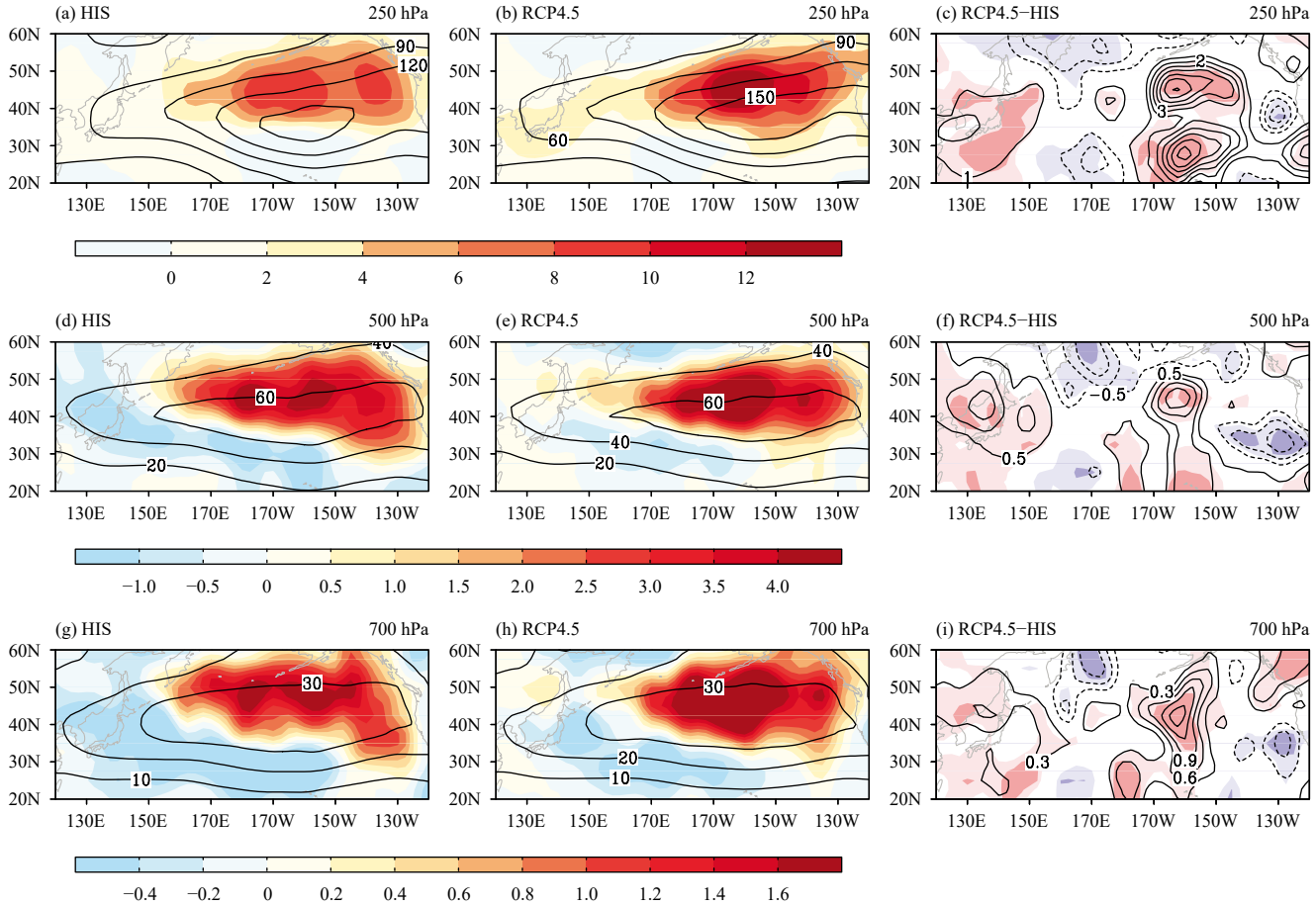

Fig. 7. As in Fig. 6, but for RCP4.5 run.

tion of the storm track (Figs. 6–8). Compared with the historical run, the regression of the near-surface baroclinicity becomes larger to the north of 40°N in the RCP runs (Figs. 10d–f). This means that the oceanic front will have a greater impact on the near-surface baroclinicity to the north of 40°N, contributing to the stronger storm-track anomalies there (Figs. 6–8). It is worth noting that the oceanic frontal impact on the near-surface baroclinicity is the largest in the RCP8.5 run (Figs. 10c, f), which may also account for its strongest impact on the storm track (Fig. 8). Therefore, the stronger impact of the oceanic front on the storm track may be partially attributed to the larger oceanic frontal impact on the near-surface baroclinicity under the climate change.

Since the near-surface baroclinicity is regulated by the meridional potential temperature gradient ($\partial\theta/\partial y$) and static stability ($N$), future changes in the oceanic frontal impact on the near-surface baroclinicity may be caused by changes in its impact on $\partial\theta/\partial y$ and N. Figure 11 displays the 6BMME of $\partial\theta/\partial y$ at 850 hPa and its anomalies regressed upon I_{OF} in each RCP run, as well as the differences in the regression between the RCP and historical runs. In each RCP run, when the oceanic front increases, the meridional potential temperature gradient intensifies in the northern part of its climatological area (Figs. 11a–c), leading to the northward enhancement of the near-surface baroclinicity (Figs. 10a–c). Compared with the historical run, the oceanic front in the RCP runs has a stronger impact on the meridional potential temperature gradient to the north of 40°N (Figs. 11d–f), which causes a larger impact on the near-surface baroclinicity (Figs. 10d–f). Comparing Figs. 10 with 11, it is clear that there is a good agreement between changes in the oceanic frontal impact on the meridional potential temperature gradient and near-surface baroclinicity. However, changes in the oceanic frontal impact on the static stability seems to hardly account for changes in the impact on the near-surface baroclinicity (figure omitted). This suggests that the larger oceanic frontal impact on the near-surface baroclinicity can be mainly explained by the stronger oceanic frontal impact on the meridional potential temperature gradient under the climate change.

However, it should be noted that in all the RCP runs, the impact of the oceanic front on the near-surface baro-

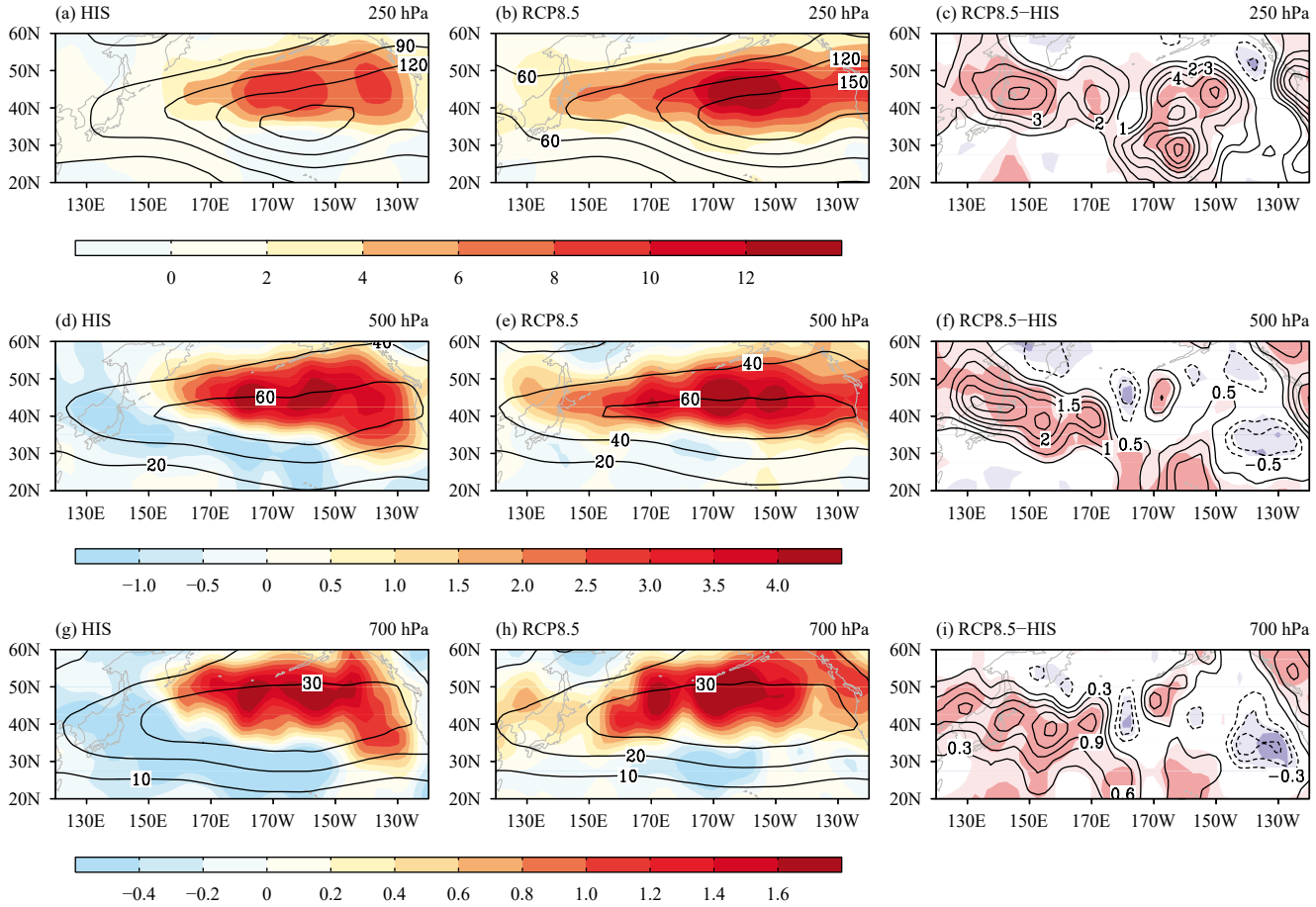

Fig. 8. As in Fig. 6, but for RCP8.5 run.

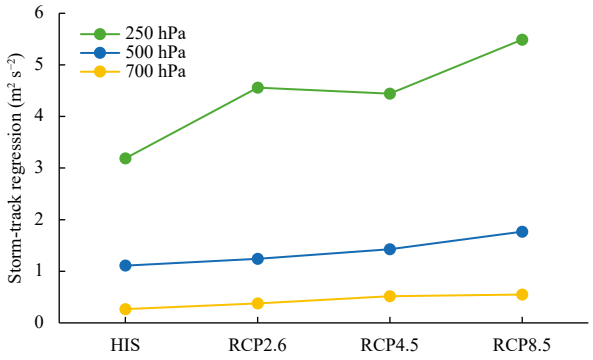

Fig. 9. The 6BMME of the storm-track regression upon I_{OF} area-averaged over 30°–50°N, 130°E–130°W ($m^2\ s^{-2}$; *y*-axis) in the historical and three RCP runs.

clinicity tends to decrease to the east of Japan (Figs. 10d–f), which seems to hardly explain the increasing impact on the storm track in the upstream (Figs. 6–8). Therefore, there may exist other potential factors that influence the relationship between the storm track and the oceanic front. Further studies are needed as it is beyond the scope of the present paper to explore other possible mechanisms.

Table 1. Rates of change (%) in the 6BMME of the storm-track regression area-averaged over 30°–50°N, 130°E–130°W in the future (2075–2099) relative to present (1980–2004) for each RCP run

	250 hPa	500 hPa	700 hPa
RCP2.6	42.94	11.86	41.50
RCP4.5	39.31	28.43	93.49
RCP8.5	72.16	59.31	106.03

5. Conclusions and discussion

In this study, the performance of 13 CMIP5 models in simulating the impact of the North Pacific midlatitude oceanic frontal intensity on the wintertime storm track is evaluated against observations, and future changes are projected based on comparisons of the multi-model ensemble of outputs of six best models (6BMME) between the three RCP runs (2075–2099) and historical run (1980–2004).

It is found that a majority of the 13 CMIP5 models can reproduce the northward intensification of the storm track when the oceanic front strengthens, and the impact of the oceanic front on the storm track is projected to get stronger and extend further westward as the radiative for-

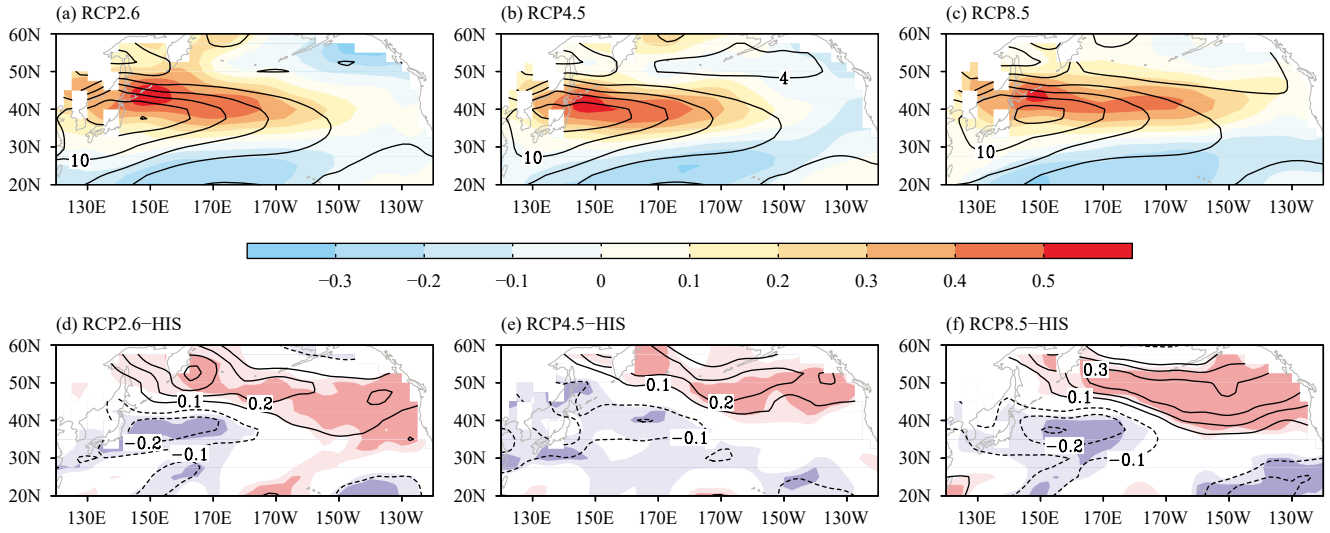

Fig. 10. The 6BMME of the wintertime near-surface baroclinicity (contour; 10^{-6} s^{-1}) and its anomalies regressed upon I_{OF} (shading; 10^{-6} s^{-1}) in the three RCP runs (upper panels) and corresponding differences in the near-surface baroclinicity regression (contour; 10^{-6} s^{-1}) between each RCP run and the historical run (lower panels). Areas shaded in red and blue denote positive and negative changes respectively, and the light (dark) shading indicates that more than three (four) of the six best models show the same sign in the projected changes.

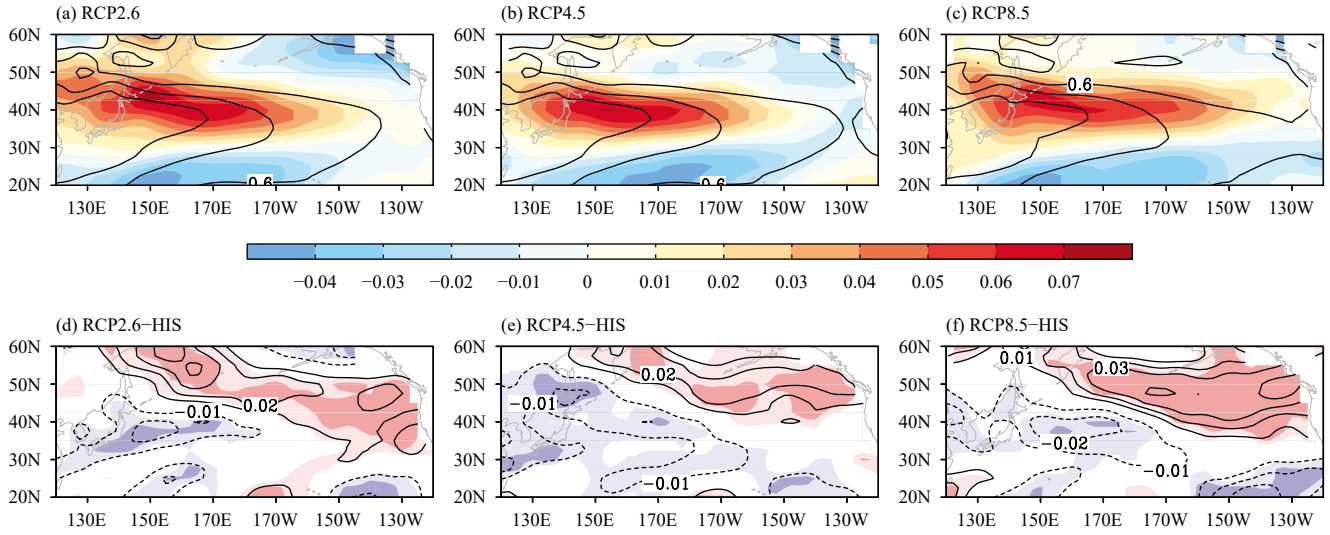

Fig. 11. As in Fig. 10, but for wintertime meridional potential temperature gradient at 850 hPa [contour; °C (100 km)$^{-1}$] and its anomalies.

cing becomes larger. Under the highest radiative forcing (RCP8.5), the storm track will increase by 106.3%, 59.3%, and 72.2% in the lower, middle, and upper troposphere, respectively. Further analysis suggests that the stronger impact of the oceanic front on the storm track may be partially attributed to the greater oceanic frontal impact on the near-surface baroclinicity, which is mainly caused by the intensified impact on the meridional potential temperature gradient in a warming climate. However, the near-surface baroclinicity anomalies can hardly explain the increasing impact on the upstream of the storm track. This study not only gives us a better understanding of future changes in the midlatitude air–sea interaction, but also helps us to predict the midlatitude climate under global warming.

Previous studies have discussed several physical mechanisms responsible for future changes in the storm track from perspectives of the horizontal atmospheric temperature gradients, upper level zonal wind, atmospheric baroclinicity, and oceanic circulation (Mizuta, 2012; Woollings et al., 2012; Harvey et al., 2014; Xiao and Zhang, 2015; Yuval and Kaspi, 2020). However, different processes may have out-of-phase influences on the storm track, leading to a tug of war on storm track responses and making future projections more difficult (Shaw et al., 2016). Hence, the processes responsible for

the future changes in the relationship between the storm track and oceanic front tend to become more complicated, and further studies are necessary to explore potential factors responsible for changes in the local response of the storm track to the oceanic front, as well as their interactions under the climate change.

Acknowledgments. The authors thank Prof. Yihui Ding and three anonymous reviewers for their constructive comments, which are helpful for us to improve the manuscript. We appreciate the World Climate Research Programme's Working Group on Coupled Modelling and the participant climate modeling groups for producing model outputs and make them available to public. The CMIP5 model outputs used in the study are downloaded from https://cmip.llnl.gov/cmip5/data_portal.html. The NCEP/NCAR Reanalysis I is available for scientific studies and the data can be downloaded from https://www.esrl.noaa.gov/psd/data/gridded/data.ncep.reanalysis.html. The HadISST1 data are obtained from the Met Office Marine Data Bank (MDB; http://www.metoffice.gov.uk/hadobs/hadisst/data/download.html).

REFERENCES

Blackmon, M. L., 1976: A climatological spectral study of the 500 mb geopotential height of the Northern Hemisphere. *J. Atmos. Sci.*, **33**, 1607–1623, doi: 10.1175/1520-0469(1976)033<1607:ACSSOT>2.0.CO;2.

Blackmon, M. L., J. M. Wallace, N.-C. Lau, et al., 1977: An observational study of the Northern Hemisphere wintertime circulation. *J. Atmos. Sci.*, **34**, 1040–1053, doi: 10.1175/1520-0469(1977)034<1040:AOSOTN>2.0.CO;2.

Booth, J. F., L. A. Thompson, J. Patoux, et al., 2010: The signature of the midlatitude tropospheric storm tracks in the surface winds. *J. Climate*, **23**, 1160–1174, doi: 10.1175/2009JCLI3064.1.

Booth, J. F., Y. O. Kwon, S. Ko, et al., 2017: Spatial patterns and intensity of the surface storm tracks in CMIP5 models. *J. Climate*, **30**, 4965–4981, doi: 10.1175/JCLI-D-16-0228.1.

Chang, E. K. M., and Y. F. Fu, 2002: Interdecadal variations in Northern Hemisphere winter storm track intensity. *J. Climate*, **15**, 642–658, doi: 10.1175/1520-0442(2002)015<0642:IVINHW>2.0.CO;2.

Chang, E. K. M., S. Lee, and K. L. Swanson, 2002: Storm track dynamics. *J. Climate*, **15**, 2163–2183, doi: 10.1175/1520-0442(2002)015<02163:STD>2.0.CO;2.

Chang, E. K. M., Y. J. Guo, and X. M. Xia, 2012: CMIP5 multimodel ensemble projection of storm track change under global warming. *J. Geophys. Res. Atmos.*, **117**, D23118, doi: 10.1029/2012JD018578.

Chang, E. K. M., C.-G. Ma, C. Zheng, et al., 2016: Observed and projected decrease in Northern Hemisphere extratropical cyclone activity in summer and its impacts on maximum temperature. *Geophys. Res. Lett.*, **43**, 2200–2208, doi: 10.1002/2016GL068172.

Chen, H. S., L. Liu, and Y. J. Zhu, 2013a: Possible linkage between winter extreme low temperature events over China and synoptic-scale transient wave activity. *Sci. China: Earth Sci.*, **42**, 1266–1280, doi: 10.1007/s11430-012-4442-z.

Chen, H. S., Y. J. Zhu, and L. Liu, 2013b: Relationship of synoptic-scale transient eddies and extreme winter precipitation events in the middle and lower reaches of the Yangtze River. *Chinese J. Atmos. Sci.*, **37**, 801–814, doi: 10.3878/j.issn.1006-9895.2012.12033. (in Chinese)

Chu, C. J., H. B. Hu, X.-Q. Yang, et al., 2020: Midlatitude atmospheric transient eddy feedbacks influenced ENSO-associated wintertime Pacific teleconnection patterns in two PDO phases. *Climate Dyn.*, **54**, 2577–2595, doi: 10.1007/s00382-020-05134-4.

Fang, J. B., and X.-Q. Yang, 2016: Structure and dynamics of decadal anomalies in the wintertime midlatitude North Pacific ocean–atmosphere system. *Climate Dyn.*, **47**, 1989–2007, doi: 10.1007/s00382-015-2946-x.

Frankignoul, C., N. Sennéchael, Y. O. Kwon, et al., 2011: Influence of the meridional shifts of the Kuroshio and the Oyashio Extensions on the atmospheric circulation. *J. Climate*, **24**, 762–776, doi: 10.1175/2010JCLI3731.1.

Gan, B. L., and L. X. Wu, 2013: Seasonal and long-term coupling between wintertime storm tracks and sea surface temperature in the North Pacific. *J. Climate*, **26**, 6123–6136, doi: 10.1175/JCLI-D-12-00724.1.

Harvey, B. J., L. C. Shaffrey, T. J. Woollings, et al., 2012: How large are projected 21st century storm track changes? *Geophys. Res. Lett.*, **39**, L18707, doi: 10.1029/2012GL052873.

Harvey, B. J., L. C. Shaffrey, and T. J. Woollings, 2014: Equator-to-pole temperature differences and the extra-tropical storm track responses of the CMIP5 climate models. *Climate Dyn.*, **43**, 1171–1182, doi: 10.1007/s00382-013-1883-9.

Huang, J., Y. Zhang, X.-Q. Yang, et al., 2020: Impacts of North Pacific subtropical and subarctic oceanic frontal zones on the wintertime atmospheric large-scale circulations. *J. Climate*, **33**, 1897–1914, doi: 10.1175/JCLI-D-19-0308.1.

Kalnay, E., M. Kanamitsu, R. Kistler, et al., 1996: The NCEP/NCAR 40-year reanalysis project. *Bull. Amer. Meteor. Soc.*, **77**, 437–472, doi: 10.1175/1520-0477(1996)077<0437:TNYRP>2.0.CO;2.

Knutti, R., D. Masson, and A. Gettelman, 2013: Climate model genealogy: Generation CMIP5 and how we got there. *Geophys. Res. Lett.*, **40**, 1194–1199, doi: 10.1002/grl.50256.

Li, R., Z. Jing, Z. H. Chen, et al., 2017: Response of the Kuroshio Extension path state to near-term global warming in CMIP5 experiments with MIROC4h. *J. Geophys. Res. Oceans*, **122**, 2871–2883, doi: 10.1002/2016JC012468.

Lindzen, R. S., and B. Farrell, 1980: A simple approximate result for the maximum growth rate of baroclinic instabilities. *J. Atmos. Sci.*, **37**, 1648–1654, doi: 10.1175/1520-0469(1980)037<1648:ASARFT>2.0.CO;2.

Ma, X. J., and Y. C. Zhang, 2018: Interannual variability of the North Pacific winter storm track and its relationship with extratropical atmospheric circulation. *Climate Dyn.*, **51**, 3685–3698, doi: 10.1007/s00382-018-4104-8.

Meinshausen, M., S. J. Smith, K. Calvin, et al., 2011: The RCP greenhouse gas concentrations and their extensions from 1765 to 2300. *Climatic Change*, **109**, 213–241, doi: 10.1007/s10584-

011-0156-z.

Mizuta, R., 2012: Intensification of extratropical cyclones associated with the polar jet change in the CMIP5 global warming projections. *Geophys. Res. Lett.*, **39**, L19707, doi: 10.1029/2012GL053032.

Moss, R. H., J. A. Edmonds, K. A. Hibbard, et al., 2010: The next generation of scenarios for climate change research and assessment. *Nature*, **463**, 747–756, doi: 10.1038/nature08823.

Nakamura, H., and A. S. Kazmin, 2003: Decadal changes in the North Pacific oceanic frontal zones as revealed in ship and satellite observations. *J. Geophys. Res. Oceans*, **108**, 3078, doi: 10.1029/1999JC000085.

Nakamura, H., T. Sampe, Y. Tanimoto, et al., 2004: Observed associations among storm tracks, jet streams and midlatitude oceanic fronts. *Earth's Climate: The Ocean–Atmosphere Interaction*, C. Wang, S. P. Xie, and J. A. Carton, Eds., American Geophysical Union, Washington DC, Book Series, Vol. 147, 329–345, doi: 10.1029/147GM18.

Nakamura, H., T. Sampe, A. Goto, et al., 2008: On the importance of midlatitude oceanic frontal zones for the mean state and dominant variability in the tropospheric circulation. *Geophys. Res. Lett.*, **35**, L15709, doi: 10.1029/2008GL034010.

Nakamura, M., and S. Yamane, 2010: Dominant anomaly patterns in the near-surface baroclinicity and accompanying anomalies in the atmosphere and oceans. Part II: North Pacific basin. *J. Climate*, **23**, 6445–6467, doi: 10.1175/2010JCLI3017.1.

Omrani, N. E., F. Ogawa, H. Nakamura, et al., 2019: Key Role of the Ocean Western Boundary currents in shaping the Northern Hemisphere climate. *Sci. Rep.*, **9**, 3014, doi: 10.1038/s41598-019-39392-y.

Pfahl, S., and H. Wernli, 2012a: Quantifying the relevance of cyclones for precipitation extremes. *J. Climate*, **25**, 6770–6780, doi: 10.1175/JCLI-D-11-00705.1.

Pfahl, S., and H. Wernli, 2012b: Quantifying the relevance of atmospheric blocking for co-located temperature extremes in the Northern Hemisphere on (sub-)daily time scales. *Geophys. Res. Lett.*, **39**, L12807, doi: 10.1029/2012GL052261.

Rayner, N. A., D. E. Parker, E. B. Horton, et al., 2003: Global analyses of sea surface temperature, sea ice, and night marine air temperature since the late nineteenth century. *J. Geophys. Res. Atmos.*, **108**, 4407, doi: 10.1029/2002JD002670.

Sampe, T., H. Nakamura, A. Goto, et al., 2010: Significance of a midlatitude SST frontal zone in the formation of a storm track and an eddy-driven westerly jet. *J. Climate*, **23**, 1793–1814, doi: 10.1175/2009JCLI3163.1.

Sanderson, B. M., R. Knutti, and P. Caldwell, 2015: A representative democracy to reduce interdependency in a multimodel ensemble. *J. Climate*, **28**, 5171–5194, doi: 10.1175/JCLI-D-14-00362.1.

Seager, R., and I. R. Simpson, 2016: Western boundary currents and climate change. *J. Geophys. Res. Oceans*, **121**, 7212–7214, doi: 10.1002/2016JC012156.

Shaw, T. A., M. Baldwin, E. A. Barnes, et al., 2016: Storm track processes and the opposing influences of climate change. *Nat. Geosci.*, **9**, 656–664, doi: 10.1038/ngeo2783.

Small, R. J., S. P. DeSzoeke, S.-P. Xie, et al., 2008: Air–sea interaction over ocean fronts and eddies. *Dyn. Atmos. Oceans*, **45**, 274–319, doi: 10.1016/j.dynatmoce.2008.01.001.

Small, R. J., R. A. Tomas, and F. O. Bryan, 2014: Storm track response to ocean fronts in a global high-resolution climate model. *Climate Dyn.*, **43**, 805–828, doi: 10.1007/s00382-013-1980-9.

Taguchi, B., H. Nakamura, M. Nonaka, et al., 2009: Influences of the Kuroshio/Oyashio Extensions on air–sea heat exchanges and storm-track activity as revealed in regional atmospheric model simulations for the 2003/04 cold season. *J. Climate*, **22**, 6536–6560, doi: 10.1175/2009JCLI2910.1.

Tamarin-Brodsky, T., and Y. Kaspi, 2017: Enhanced poleward propagation of storms under climate change. *Nat. Geosci.*, **10**, 908–913, doi: 10.1038/s41561-017-0001-8.

Taylor, K. E., R. J. Stouffer, and G. A. Meehl, 2012: An overview of CMIP5 and the experiment design. *Bull. Amer. Meteor. Soc.*, **93**, 485–498, doi: 10.1175/BAMS-D-11-00094.1.

Van Vuuren, D. P., J. Edmonds, M. Kainuma, et al., 2011: The representative concentration pathways: An overview. *Climatic Change*, **109**, 5–31, doi: 10.1007/s10584-011-0148-z.

Wang, L. Y., H. B. Hu, and X.-Q. Yang, 2019: The atmospheric responses to the intensity variability of subtropical front in the wintertime North Pacific. *Climate Dyn.*, **52**, 5623–5639, doi: 10.1007/s00382-018-4468-9.

Wettstein, J. J., and J. M. Wallace, 2010: Observed patterns of month-to-month storm-track variability and their relationship to the background flow. *J. Atmos. Sci.*, **67**, 1420–1437, doi: 10.1175/2009JAS3194.1.

Woollings, T., J. M. Gregory, J. G. Pinto, et al., 2012: Response of the North Atlantic storm track to climate change shaped by ocean–atmosphere coupling. *Nat. Geosci.*, **5**, 313–317, doi: 10.1038/ngeo1438.

Xiao, C. L., and Y. C. Zhang, 2015: Projected changes of wintertime synoptic-scale transient eddy activities in the East Asian eddy-driven jet from CMIP5 experiments. *Geophys. Res. Lett.*, **42**, 6008–6013, doi: 10.1002/2015GL064641.

Yang, H., G. Lohmann, W. Wei, et al., 2016: Intensification and poleward shift of subtropical western boundary currents in a warming climate. *J. Geophys. Res. Oceans*, **121**, 4928–4945, doi: 10.1002/2015JC011513.

Yao, Y., Z. Zhong, and X.-Q. Yang, 2016: Numerical experiments of the storm track sensitivity to oceanic frontal strength within the Kuroshio/Oyashio extensions. *J. Geophys. Res. Atmos.*, **121**, 2888–2900, doi: 10.1002/2015JD024381.

Yao, Y., Z. Zhong, X.-Q. Yang, et al., 2017: An observational study of the north pacific storm-track impact on the midlatitude oceanic front. *J. Geophys. Res. Atmos.*, **122**, 6962–6975, doi: 10.1002/2016JD026192.

Yao, Y., Z. Zhong, X.-Q. Yang, et al., 2018a: Seasonal variation of the North Pacific storm-track relationship with the Subarctic frontal zone intensity. *Dyn. Atmos. Oceans*, **83**, 75–82, doi: 10.1016/j.dynatmoce.2018.06.003.

Yao, Y., Z. Zhong, and X.-Q. Yang, 2018b: Impacts of the subarctic frontal zone on the North Pacific storm track in the cold season: An observational study. *Int. J. Climatol.*, **38**, 2554–2564, doi: 10.1002/joc.5429.

Yao, Y., Z. Zhong, X.-Q. Yang, et al., 2019: Seasonal variations of the relationship between the North Pacific storm track and the meridional shifts of the subarctic frontal zone. *Theor. Appl. Climatol.*, **136**, 1249–1257, doi: 10.1007/s00704-018-2559-5.

Yin, J. H., 2005: A consistent poleward shift of the storm tracks in

simulations of 21st century climate. *Geophys. Res. Lett.*, **32**, L18701, doi: 10.1029/2005GL023684.

Yuan, L., and Z. N. Xiao, 2017: The variability of the oceanic front in Kuroshio Extension and its relationship with the Pacific storm track in winter. *Chinese J. Atmos. Sci.*, **41**, 1141–1155, doi: 10.3878/j.issn.1006-9895.1705.16276. (in Chinese)

Yuval, J., and Y. Kaspi, 2020: Eddy activity response to global warming-like temperature changes. *J. Climate*, **33**, 1381–1404, doi: 10.1175/JCLI-D-19-0190.1.

Zhang, X., Q. Wang, and M. Mu, 2017: The impact of global warming on Kuroshio Extension and its southern recirculation using CMIP5 experiments with a high-resolution climate model MIROC4h. *Theor. Appl. Climatol.*, **127**, 815–827, doi: 10.1007/s00704-015-1672-y.

Zhang, Y. X., and Y. H. Ding, 2014: A study of simulation and prediction of extratropical cyclones over the Northern Hemisphere part II: Future changes under RCP4.5 projected by the 6 CMIP5 coupled models. *Acta Meteor. Sinica*, **72**, 1171–1185, doi: 10.11676/qxxb2014.073. (in Chinese)

Zhou, X. Y., W. J. Zhu, and C. Gu, 2015: Possible influence of the variation of the northern Atlantic storm track on the activity of cold waves in China during winter. *Chinese J. Atmos. Sci.*, **39**, 978–990, doi: 10.3878/j.issn.1006-9895.1501.14259. (in Chinese)

Tech & Copy Editor: Meili ZHANG